Results in Physics 29 (2021) 104692

Contents lists available at ScienceDirect

Results in Physics

journal homepage: www.elsevier.com/locate/rinp

Interfacial electronic structure at rubrene/NiFe heterostructure

ARTICLE INFO

Keywords
Permalloy
Rubrene
Photoemission spectroscopy
Electronic structure

ABSTRACT

The interface electronic structure between rubrene and permalloy ($Ni_{80}Fe_{20}$) has been studied by ultraviolet photoelectron spectroscopy (UPS) and X-ray photoelectron spectroscopy (XPS). We find that the downward energy level bending at the rubrene/NiFe heterostructure is caused by the interaction between rubrene and NiFe at the interface. There is an interface dipole of 0.23 eV, pointing from NiFe to rubrene. Our researches deepen the understanding of the fundamentals and laid a foundation for the design of high-performance rubrene-based organic spintronic devices.

Introduction

Organic semiconductors (OSC) with hyperfine interaction and weak spin orbit coupling have been extensively pursued for many applications such as organic photovoltaics (OPVs), organic light-emitting diodes (OLEDs), and organic field effect transistors (OFETs) [1–8]. The research of organic spintronic devices based on various organic materials like Alq_3, PEDOT, C_{60} was reported successively [9–12]. In 2002, Dediu reported a magnetoresistance (MR) of nearly 30 % at room temperature in first lateral spin valve by using sexithienyl molecule as the spacer and $La_{0.7}Sr_{0.3}MnO_3$ (LSMO) as the electrodes [13]. Xiong *et al.* prepared the first vertical organic spin valve device based on Co/Alq_3/LSMO structure in 2004, and got an MR of nearly 40 % at low temperature [14]. Cinchetti *et al.* found that the efficiency of spin injection at cobalt-CuPc interface is 85–90 % [15]. Gobbi *et al.* obtained an MR of more than 5 % at room temperature in Co/AlO_x/C_{60}/NiFe devices [16]. TVAG team found an upper limit for the spin lifetime of carriers in PEDOT:PSS nanoscale lateral devices, and its value is about 50 ns [17].

Rubrene has been applicated in OPVs, OLEDs and OFETs widely for its stable molecular structure, low band gap and relatively high carriers transfer rate [18–20]. Podzorov *et al.* found that the hole mobility is 20 cm^2/Vs at room temperature in the organic thin-film transistor by using rubrene single crystal [21]. Zhang *et al.* reported an MR ratio of approximately 6 % at room temperature in organic spin valves with a Fe_3O_4/AlO/rubrene/Co stacking structure [22]. NiFe is often used as the ferromagnetic electrode for organic spintronic devices due to its high spin polarization and Curie temperature [23–27]. Sun team reported a spin photovoltaic device with a NiFe/C_{60}/Co structure, which can be widely used in sensors and magnetic current converters [28]. Alqahtani *et al.* fabricated a planar organic spin valve with a PTCDI-C_{13}/NiFe structure, and they obtained an MR ratio of 0.35 % at room temperature [29]. Liu *et al.* reported a longest spin diffusion length in NiFe/fullerene/Pt device when the thickness of C_{70} is 25 nm [30]. Li *et al.* fabricated a device with a NiFe/rubrene/Pt structure and found that the spin diffusion length is 132 nm and the spin relaxation time is 3.8 ms at room temperature [31]. It is well known that the carriers will inevitably pass through the interface between rubrene and metal electrode in rubrene-based devices. The performance and characteristics of rubrene-based devices are usually significantly affected by the interface electronic structure. Such as, Ding *et al.* found that interface dipoles are formed at interfaces with Au, Ag, and Al due to charge transfer between rubrene molecule and the metal substrates [32]. Therefore, it is of great significance to study the interface electronic structure at the rubrene/metal interface, which is conducive to the preparation of spin related devices [33,34].

In this paper, we report our investigations on the electronic structure of rubrene/NiFe heterostructure interface using photoemission spectroscopy (PES). A 0.23 eV interface dipole was observed at the rubrene/NiFe interface. We found that the interface interactions at the interface between rubrene and NiFe can lead to the downward energy level bending.

Experimental section

Sample Preparation: We performed the vapor deposition and photoelectron spectroscopy (PES) in a ultrahigh vacuum system which consisting of magnetron sputtering chamber, organic growth chamber, spectrometer chamber with base pressure of 1×10^{-8} mbar, 2×10^{-9} mbar, 2×10^{-10} mbar, respectively, as described previously [35–37]. MgO (1 0 0) was annealed in oxygen atmosphere for 30 min at a temperature of 450 ℃. NiFe film was deposited on MgO (1 0 0) substrate by RF magnetron sputtering and its thickness is about 35 nm. As shown in Fig. 1(b), rubrene were thermal evaporated at deposition rate of 1 Å/min and its thickness is 2, 4, 8, 16, 32 and 64 Å respectively [38,39]. Quartz Crystal Microbalance (QCM) was used to monitor the thickness of rubrene film.

Photoelectron Spectroscopy: The spectrometer chamber is mainly composed of a hemispherical energy analyzer, a microwave UV light source (He I = 21.22 eV) and a monochromatic X-ray source (Al Kα = 1486.7 eV). The diameter of UV spot is about 1 mm [40]. The total energy resolution test obtained by measuring the Fermi edge of a clean polycrystalline Au at room temperature and a total instrumental energy resolution of 70 meV is obtained. The secondary cut-off edge was obtained under negative 5 V bias in UPS measurements. All measurements

https://doi.org/10.1016/j.rinp.2021.104692
Received 21 April 2021; Received in revised form 11 August 2021; Accepted 11 August 2021
Available online 17 August 2021

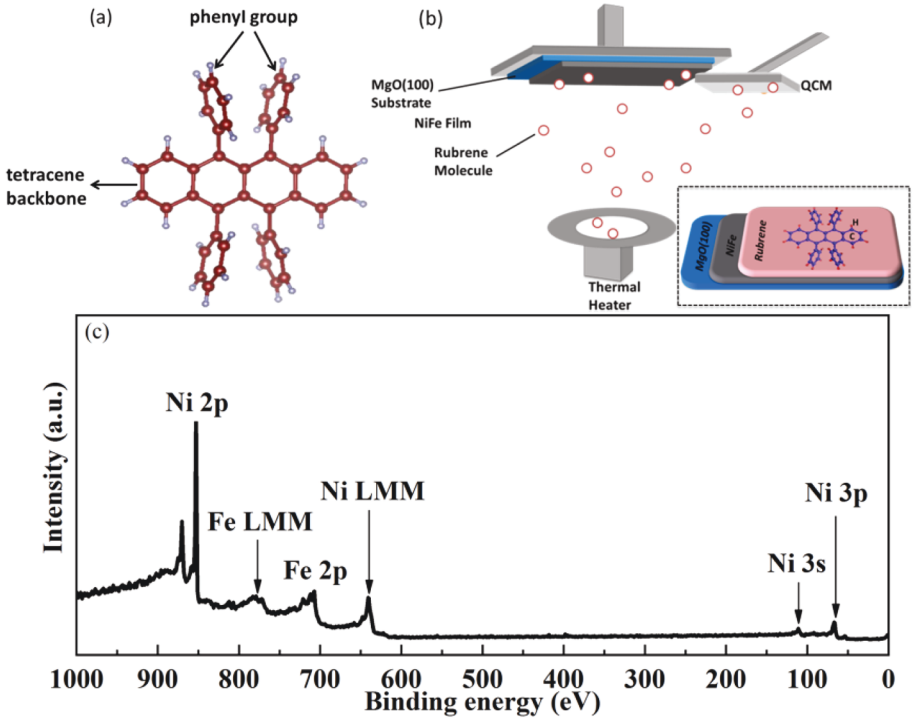

Fig. 1. (a) Molecular structure of rubrene. (b) Schematic diagram of the rubrene deposited on permalloy ($Ni_{80}Fe_{20}$) which was grown on MgO (1 0 0) substrate. (c) XPS full spectra of NiFe substrate.

were taken at room temperature.

Results and discussion

In Fig. 1, the molecular structure and schematic diagram of the evaporation of rubrene are presented. Rubrene is made up of tetracene backbone and four phenyl groups, as shown in Fig. 1(a). The four phenyl are rotated out of the plane of the tetracene backbone owing to steric hindrance. For the intrinsic rubrene, the spectral features closer to the valence band edge can be attributed to the contribution of the tetracene backbone [41,42]. The remaining part of the spectrum at higher binding energy are dominated by both the tetracene backbone and phenyl groups [43]. Fig. 1(b) present the schematic representation of rubrene deposited on NiFe/MgO(1 0 0) by thermal evaporation. Fig. 1(c) shows the XPS full spectra of NiFe substrate. The sample displays only nickel and iron, indicating that the surface of the NiFe film is clean.

Fig. 2 shows the UPS spectra of the stepwise deposition of rubrene on NiFe substrate. In order to have a more intuitive and clear vision, we normalized the intensity of the spectrum to the [0, 1] interval by the Origin software. In Fig. 2(a), the work function (WF) is 5.03 eV before

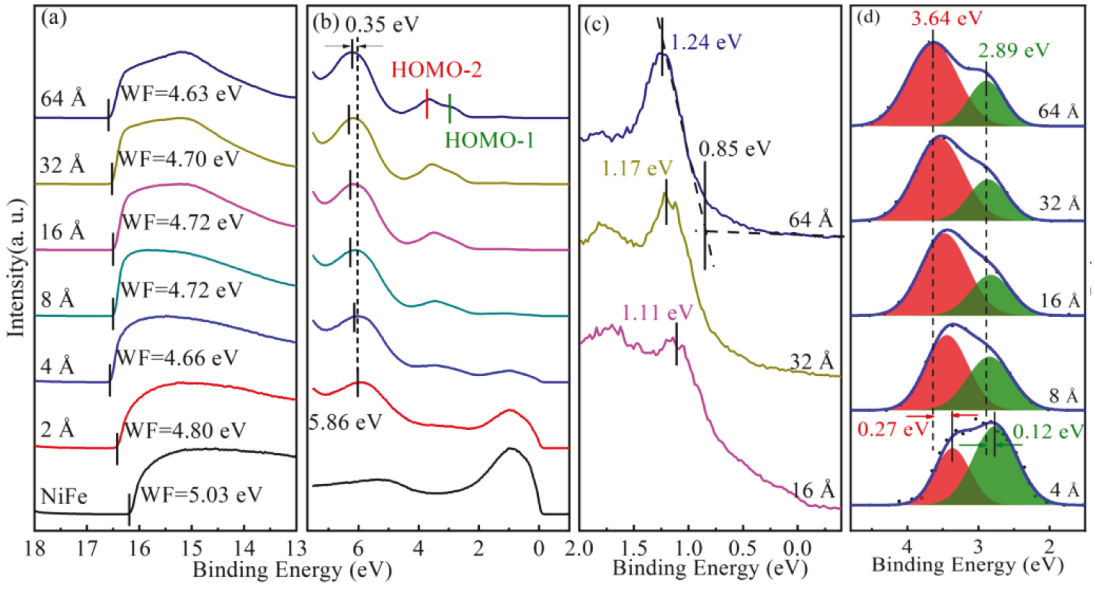

Fig. 2. Evolution of UPS spectra as a function of rubrene thickness. (a) Cut-off region, (b) HOMO region, (c) Magnified at binding energy between −0.4 eV to 2 eV. (d) Evolutions of the HOMO-1 (green peak) and HOMO-2 (red peak) as the rubrene thickness increases. (For interpretation of the references to colour in this figure legend, the reader is referred to the web version of this article.)

rubrene deposition. After the deposition of rubrene, the WF decreases to 4.66 eV at 4 Å and the total shift is about 0.37 eV. Then the WF increases to 4.72 eV at 8 Å and decreases to 4.63 eV with further increasing of the rubrene thickness, the total shift is about 0.09 eV. The WF decrease quickly at lower rubrene coverage (from 0 to 4 Å) can be attribute to interface interaction at rubrene/NiFe interface, which lead to a discontinuous change of WF as the rubrene thickness increases. Fig. 2(b) and 2(c) presents the evolution of the HOMO region as the increasing of rubrene thickness. The HOMO onsets are obtained by linear extrapolation as previously illustrated [44–46]. In Fig. 2(b), two peaks at higher binding energy region (2–5 eV), marked as HOMO-1 and HOMO-2 respectively, are dominated by both the tetracene backbone and phenyl groups [43]. Shown in Fig. 2(c) are the magnification of HOMO region lower than 2 eV, which is dominated by the contributions from the tetracene backbone and plays an important role in its transport properties [41,42]. The HOMO onset of 64 Å rubrene is located at about 0.85 eV below the Fermi level. As shown in Fig. 2(d), the HOMO-1 and HOMO-2 peaks are fitted with fixed width after a Shirley background correction. As the increasing of rubrene thickness, the intensity of the HOMO-2 peak (red peak) increases while the HOMO-1 peak (green peak) decreases. The change of HOMO-1 and HOMO-2 peaks can be attributed to the interfacial interaction at rubrene/NiFe interface, which is consistent with previous reports in the literature [47].

To better understand the interfacial interaction between rubrene and NiFe, the chemical characteristics were investigated by using XPS. The C 1s core level can be fitted by two peaks, as shown in Fig. 3(a). The peak located at about 285.29 eV (C–C) can be assigned to the intrinsic peak of rubrene and that located at about 285.47 eV (rubrene-NiFe) is usually related to interfacial interaction [48]. It is find that the rubrene-NiFe peak decreases as the increasing of rubrene thickness, indicated that the interfacial interaction mainly exist in the rubrene/NiFe heterojunction interface. Fig. 3(b) show the change of Ni $2p_{3/2}$ core level with the increasing of rubrene thickness. We can see that the position of the Ni $2p_{3/2}$ from the NiFe substrate does not shift and no peak or shoulder is detected at around 852.78 eV. It indicates that the NiFe substrate is not affected appreciably by the rubrene film. In Fig. 3(c), the ratio of rubrene-NiFe/C–C decreases dramatically at the initial rubrene deposition stage (<8 Å) and decreases gradually with further increasing the rubrene thickness, indicating the existence of interfacial interaction at the rubrene/NiFe heterojunction interface.

The energy levels diagram at the rubrene/NiFe interface is shown in Fig. 4. According to the previous test results, the energy band gap of rubrene is 2.67 eV [32]. There is an interfacial dipole of 0.23 eV pointing

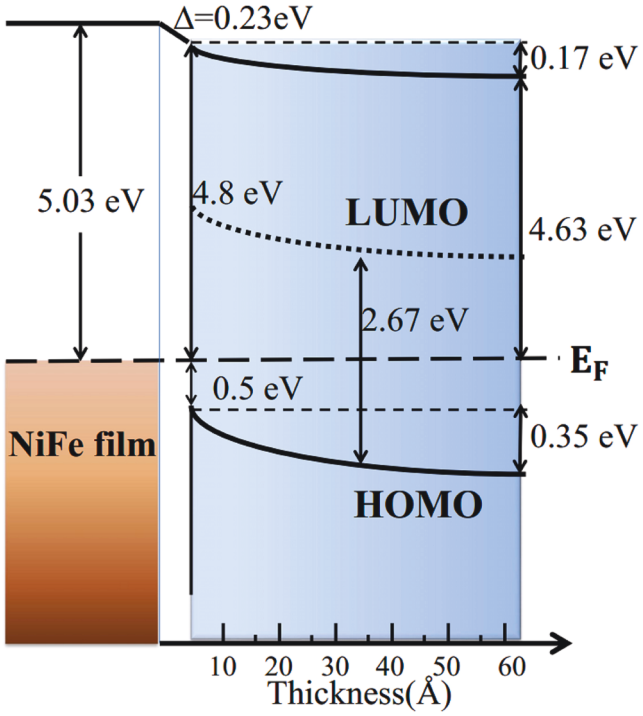

Fig. 4. The energy levels diagram at the rubrene/NiFe interface.

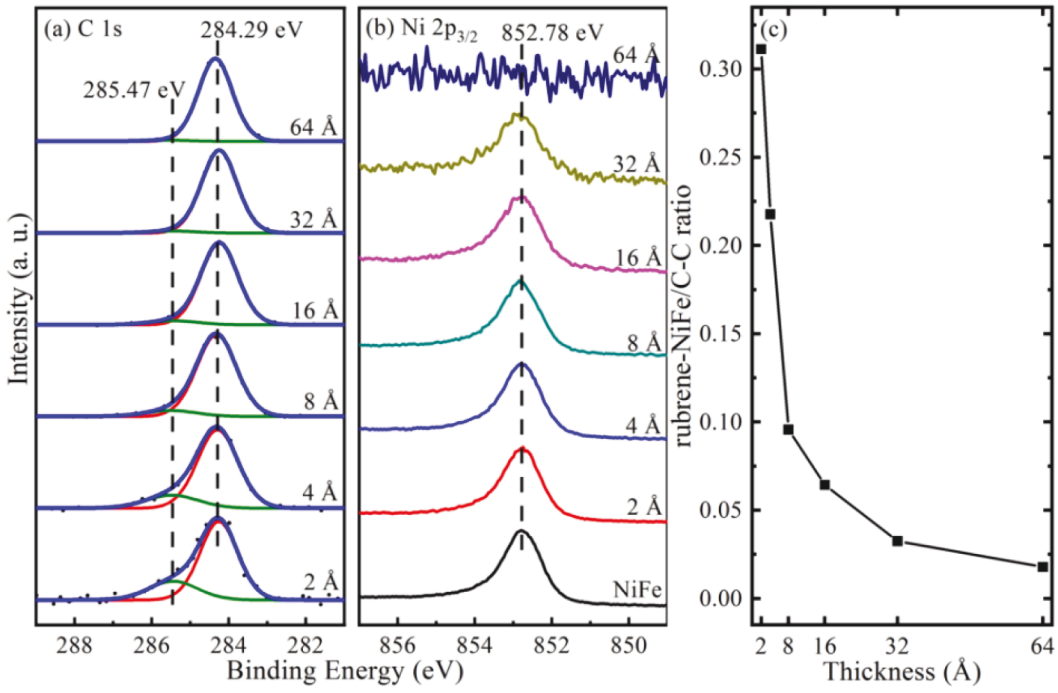

Fig. 3. Evolution of XPS spectra as a function of rubrene thickness. (a) C 1s, (b) Ni $2p_{3/2}$ (c) The ratio of rubrene-NiFe to C–C.

from NiFe to rubrene. The existence of interfacial interaction leads to the downward energy level bending. As we all know, there are many reasons for the formation of energy level bending, such as interface charge transfer, charging phenomenon, interfacial chemical reaction and so on [49–52]. It can be observed from Fig. 4 that the Fermi level of NiFe is almost in the middle region between the HOMO and LUMO of rubrene. It indicated that there is no interfacial charge transfer [53]. We can exclude the charging phenomenon because the C 1s core level does not shift as the rubrene thickness increases, as shown in Fig. 3(a). We also found that the position of Ni $2p_{3/2}$ keeps unchanged, indicates that no interfacial chemical reaction has occurred at rubrene/NiFe interface. Fig. 2(d) show that the interfacial interaction affects the intensity of the two HOMO (HOMO-1, HOMO-2) peaks. The change of rubrene-NiFe/C–C ratio further indicates that there is an interfacial interaction at the rubrene/NiFe heterojunction interface.

Conclusions

In conclusion, the electronic structure of rubrene/NiFe interface had been investigated by using UPS and XPS. We find that the interfacial interaction between rubrene and NiFe leads to the downward energy level bending. The interfacial dipole pointing from NiFe to rubrene is 0.23 eV. These observations provide important information to design high-performance rubrene/NiFe-based organic spintronic devices.

Declaration of Competing Interest

The authors declare that they have no known competing financial interests or personal relationships that could have appeared to influence the work reported in this paper.

Acknowledgments

P. Y. and Y.L. contributed equally to this work. We thank the financial support by the National Natural Science Foundation of China (Grant Nos. 51802355) and National Key Research and Development Program of China (Grant Nos. 2017YFA0206602). H.X. acknowledges the support by the Natural Science Foundation of Hunan Province (Grant No. 2018JJ3625) and the Innovation-Driven Project of Central South University (2020CX006). Y.G. acknowledges the support by the National Science Foundation (Grant Nos. DMR-1903981 and 1903962).

References

[1] Fillaud L, Petenzi T, Pallu J, Piro B, Mattana G, Noel V. Switchable hydrogel-gated organic field effect transistors. Langmuir 2018;34:3686–93.
[2] Meier G, Matsuyama T, Merkt U. Field effect in InAs/permalloy hybrid transistors. Phys Rev B 2002;65:125327.
[3] Gardelis S, Smith CG, Barnes CHW, Linfield EH, Ritchie DA. An observation of spin-valve effects in a semiconductor field effect transistor: a novel spintronic device. Phys Rev B 2012;11:679–91.
[4] Vassilakopoulou A, Papadatos D, Zakouras I, Koutselas I. Mixtures of quasi-two and three dimensional hybrid organic-inorganic semiconducting perovskites for single layer LED. J Alloy Compd 2016;692:589–98.
[5] Manago T, Akinaga H. Spin-polarized light-emitting diode using metal/insulator/semicond- uctor structures. Appl Phys Lett 2002;81:694–8.
[6] Fiederling R, Keim M, Reuscher G, Ossau W, Schmidt G, Waag A, et al. Injection and detection of a spin-polarized current in a light-emitting diode. Nature 1999;402:787–90.
[7] Oseni SO, Kaviyarasu K, Maaza M, Sharma G, Pellicane G, Mola GT. ZnO:CNT assisted charge transport in PTB7:PCBM blend organic solar cell. J Alloy Compd 2018;748:216–22.
[8] Dong HS, Sang WS, Kim JM, Lee HS, Choi SH. Graphene transparent conductive electrodes doped with graphene quantum dots-mixed silver nanowires for highly-flexible organic solar cells. J Alloy Compd 2018;744:1–6.
[9] Barraud C, Seneor P, Mattana R, Fusil S, Bouzehouane K, Deranlot C. Unravelling the role of the interface for spin injection into organic semiconductors. Nat Phys 2010;6:615–20.
[10] Kawasugi Y, Ara M, Ushirokita H, Kamiya T, Tada H. Preparation of lateral spin-valve structure using doped conducting polymer poly(3,4-ethylenedioxythiophene) poly(styrenesulfonate). Org Electron 2013;14:1869–73.
[11] Liu HL, Wang JY, Groesbeck M, Pan X, Zhang C, Vardeny ZV. Studies of spin related processes in fullerene C_{60} devices. J Mater Chem C 2018;6:3621–7.
[12] Majumdar S, Majumdar HS, Laiho R, Österbacka R. Comparing small molecules and polymer for future organic spin-valves. J Alloy Compd 2006;423:169–71.
[13] Dediu V, Murgia M, Matacotta FC, Taliani C, Barbanera S. Room temperature spin polarized injection in organic semiconductor. Solid State Commun 2002;122:181–4.
[14] Xiong ZH, Wu D, Vardeny ZV, Jing S. Giant magnetoresistance in organic spin-valves. Nature 2004;427:821–4.
[15] Cinchetti M, Heimer K, Wüstenberg JP, Andreyev O, Bauer M, Lach S. Determination of spin injection and transport in a ferromagnet/organic semiconductor heterojunction by two-photon photoemission. Nat Mater 2009;8:115–9.
[16] Gobbi M, Golmar F, Llopis R, Casanova F, Hueso LE. Room-temperature spin transport in C_{60}-based spin valves. Adv Mater 2011;23:1609–13.
[17] Oliveira TD, Gobbi M, Porro JM, Hueso LE, Bittner AM. Charge and spin transport in PEDOT:PSS nanoscale lateral devices. Nanotechnology 2013;24:475201.
[18] Saikia D, Sarma R. Characterization of organic light-emitting diode using a rubrene interlayer between electrode and hole transport layer. Bull Mater Sci 2020;43:35–43.
[19] Su WC, Lee CC, Li YZ, Liu SW. The influence of singlet and charge-transfer excitons on the open-circuit voltage of rubrene/fullerene organic photovoltaic device. ACS Appl Mater Interfaces 2016;8:28757–62.
[20] Ohmi SI, Hiroki M, Park KE, Maeda Y. Scaling of top-gate/bottom-contact pentacene-based organic field-effect transistors with amorphous rubrene gate insulator. Jpn J Appl Phys 2019;58:SBBG01.
[21] Podzorov V, Menard E, Borissov A, Kiryukhin V, Rogers JA, Gershenson ME. Intrinsic charge transport on the surface of organic semiconductors. Phys Rev Lett 2004;93:086602.
[22] Zhang X, Ma Q, Suzuki K, Sugihara A, Qin G, Miyazaki T. Magnetoresistance effect in rubrene-based spin valves at room temperature. Acs Appl Mater Interfaces 2015;7:4685–92.
[23] Tanaka T, Ohtake M, Kirino F, Futamoto M. Microstructure of NiFe epitaxial thin films grown on MgO single-crystal substrates. IEEE Trans Magn 2010;46:345–8.
[24] Yu JH, Lee HM, Ando Y, Miyazaki T. Electron transport properties in magnetic tunnel junctions with epitaxial NiFe(111) ferromagnetic bottom electrodes. Appl Phys Lett 2003;82:4735–7.
[25] Zhang H, Desai P, Zhan YQ, Drew AJ, Kreouzis T. The importance of holes in aluminium tris-8-hydroxyquinoline (Alq3) devices with Fe and NiFe contacts. Appl Phys Lett 2014;104:013303.
[26] Vavassori P, Gobbi M, Pascual A, Golmar F, Hueso LE. C_{60}/NiFe combination as a promising platform for molecular spintronics. Org Electron 2012;13:366–72.
[27] Mugadza K, Nyamori VO, Mola GT, Simoyi RH, Ndungu PG. Low temperature synthesis of multiwalled carbon nanotubes and incorporation into an organic solar cell. J Exp Nanosci 2017;1357842:1–21.
[28] Sun X, Vélez S, Atxabal A, Bedoya-Pinto A, Parui S, Zhu XW. A molecular spin-photovoltaic device. Science 2017;357:677–80.
[29] Alqahtani H, Bryan MT, Hayward TJ, Hodges MP, Im MY, Fischer P. Planar organic spin valves using nanostructured $Ni_{80}Fe_{20}$ magnetic contacts. Org Electron 2014;15:276–80.
[30] Liu HL, Wang JY, Chanana A, Vardeny ZV. Studies of spin transport in fullerene films. J Appl Phys 2019;125:142908.
[31] Li ZH, Li T, Qi DC, Tong W, Xiong Y. Quantitative study of spin relaxation in rubrene thin films by inverse spin hall effect. Appl Phys Lett 2019;115:053301.
[32] Ding H, Gao Y. Electronic structure at rubrene metal interfaces. Appl Phys A Mater Sci Process 2009;a95:89–94.
[33] Braun S, Salaneck WR, Fahlman M. Energy-level alignment at organic/metal and organic/organic interfaces. Adv Mater 2009;21:1450–72.
[34] Ishii H, Hayashi N, Ito E, Washizu Y, Sugi K, Kimura Y, et al. Kelvin probe study of band bending at organic semiconductor/metal interfaces: examination of fermi level alignment. Phys Status Solidi 2004;201:1075–94.
[35] Xie HP, Liu XL, Lyu L, Niu DM, Wang Q, Huang JS, et al. Effects of precursor ratios and annealing on electronic structure and surface composition of $CH_3NH_3PbI_3$ perovskite films. J Phys Chem C 2016;120:215–20.
[36] Xie HP, Niu DM, Lyu L, Zhang H, Zhang YH, Liu P, et al. Evolution of the electronic structure of $C_{60}/La_{0.67}Sr_{0.33}MnO_3$ interface. Appl Phys Lett 2016;108:011603.
[37] Xie HP, Huang H, Cao NT, Zhou CH, Niu DM, Gao YL. Effects of annealing on structure and composition of LSMO thin films. Phys B 2015;477:14–9.
[38] Blüm MC. Supramolecular assembly, chirality, and electronic properties of rubrene studied by STM and STS. École Polytechnique Federale De Lausanne 2006;157:3487.
[39] Kowert BA, Dang NC, Sobush KT, Seele LG. Diffusion of aromatic hydrocarbons in n-Alkanes and cyclohexanes. J Phys Chem A 2001;105:1232–7.
[40] Liu BX, Xie HP, Niu DM, Huang H, Wang C, Wang ST, et al. Interface electronic structure between Au and black phosphorus. J Phys Chem C 2018;122:3146.
[41] Harada Y, Takahashi T, Fujisawa S, Kajiwara T. Application of photoelectron spectroscopy to the study of photochemical reactions of solids. photooxidation of rubrene (5,6,11,12-tetraphenylnaphthacene). Chem Phys Lett 1979;62:283–6.
[42] Filho D, Kim EG, Bredas JL. Transport properties in the rubrene crystal: electronic coupling and vibrational reorganization energy. Adv Mater 2005;17:1072–6.
[43] Cheng CP, Li TL, Kuo CH, Pi TW. Electronic structures of pristine and potassium-doped rubrene thin films. Org Electron 2013;14:942–50.
[44] Liu XL, Wang CG, Irfan I, Yi SJ, Gao YL. Effect of oxygen plasma treatment on air exposed MoO_x thin film. Org Electron 2014;15:977–83.
[45] Liu XL, Wang CG, Wang CC, Irfan, Gao YL, Interfacial electronic structures of buffer-modified pentacene/C60-based charge generation layer. Organic Electronics. 2015, 17, 325-333.

[46] Zhang YH, Niu DM, Lyu L, Xie HP, Gao YL. Adsorption, film growth, and electronic structures of 2,7-dioctyl[1]benzothieno-[3,2-b][1]benzothiophene(C8-BTBT) on Cu (100). Acta Phys Sinica 2016;65:157901.
[47] Wang L, Chen S, Liu L, Qi D, Gao X, Wee ATS. Thickness-dependent energy level alignment of rubrene adsorbed on Au(111). Appl Phys Lett 2007;90:132121.
[48] Wang H, Wong SP, Cheung WY, Ke N, Wen GH, Zhang XX. Magnetic properties and structure evolution of amorphous Co-C nanocomposite films prepared by pulsed filtered vacuum arc deposition. J Appl Phys 2000;88:4919–21.
[49] Zhong JQ, Mao HY, Wang R, Qi DC, Cao L, Wang YZ, et al. Effect of gap states on the orientation- dependent energy level alignment at the DIP/F16CuPc donor-acceptor heterojunction interfaces. J Phys Chem C 2011;115:23922–8.
[50] Peisert H, Knupfer M, Schwieger T. Full characterization of the interface between the organic semiconductor copper phthalocyanine and gold. J Appl Phys 2002;91:4872–8.
[51] Salaneck WR. Intermolecular relaxation energies in anthracene. Phys Rev Lett 1978;40:60–3.
[52] Yamane H, Yabuuchi Y, Fukagawa H, Kera S, Okudaira KK, Ueno N. Does the molecular orientation induce an electric dipole in Cu-phthalocyanine thin films? J Appl Phys 2006;99:605.
[53] Braun S, Salaneck WR, Fahlman M. Energy-level alignment at organic/metal & organic/ organic interfaces basic material properties of semiconducting. Adv Mater 2009;21:1450–72.

Pan Yuan[a,1], Yuquan Liu[a,1], Haipeng Xie[a,*], Junhua Wei[a], Yuan Zhao[a], Shitan Wang[a], Yangyang Zhang[a], Dongmei Niu[a], Yongli Gao[b]
[a] *Institute of Super-Microstructure and Ultrafast Process in Advance Materials, School of Physic and Electronics, Central South University, Changsha, Hunan 410012, China*
[b] *Department of Physics and Astronomy, University of Rochester, Rochester, NY 14627, United States*

[*] Corresponding author.
E-mail address: xiehaipeng@csu.edu.cn (H. Xie).

[1] These authors contributed equally to this work.